

High Cycle Fatigue Damage Mechanisms of MAR-M 247 Superalloy at High Temperatures

M. Šmíd^{1,2}  · V. Horník^{1,3} · P. Hutař¹ · K. Hrbáček⁴ · L. Kunz¹

Received: 30 October 2015 / Accepted: 9 December 2015 / Published online: 7 January 2016
© The Indian Institute of Metals - IIM 2016

Abstract High cycle fatigue tests of the MAR-M 247 superalloy under constant load were conducted with the aim to determine S–N curves at temperatures 650, 800, 900 and 950 °C. It has been found that the slope of the S–N curves reflects changes of the cyclic deformation mechanism with temperature. At temperatures 650 and partly at 800 °C, fatigue crack propagation exhibits crystallographic character (propagation along the {111} system) in early stages of the fatigue life. The crystallographic mode of the fatigue crack propagation was found to disappear at temperatures 900 and 950 °C.

Keywords High cycle fatigue · S–N curves · Fractography · High temperature · EBSD analysis

1 Introduction

Nickel-based superalloy MAR-M 247 belongs among to the advanced cast polycrystalline materials used for turbine blades and discs, turbochargers and numerous other applications. Hence, the detailed knowledge of its resistance to the High cycle fatigue (HCF) loading is of utmost importance for its safe engineering application.

Although the alloy is known already for the last few decades and though a large amount of investigations were conducted with the aim to characterize the microstructure [1], behaviour under creep loading [2], low cycle fatigue loading [3], thermomechanical loading [4], or after processing enhancements [5] which are of great interest for industry are still not well described and understood. One of them is HCF behaviour and characterization of fatigue damage mechanisms in relation to temperature. Previous works [3, 6] brought partial results, however not in the sufficient extent and temperature range.

The aim of this work is to provide HCF experimental data at temperature range from 650 to 950 °C under conditions of constant stress amplitude and fully reversed loading. Subsequently, the description of the fatigue crack initiation and propagation mechanisms was the main focus.

2 Experimental

The superalloy MAR-M 247 was provided by the company PBS Velká Bíteš, a.s. as pre-cast rods from which specimens were machined. The chemical composition of the alloy was the following (in wt%): 0.15 C, 8.37 Cr, 0.67 Mo, 5.42 Al, 1.01 Ti, 3.05 Ta, 9.92 W, 9.91 Co, 0.04 Nb, 0.015 Br, 1.37 Hf, bal. Ni. The temperature at pouring into the mold was 1400 ± 15 °C. The material underwent hot isostatic pressing (HIP) procedure (1200 °C/4 h, 100 MPa). Subsequently, the alloy was heat treated by 2 steps, namely by solution annealing at 1200 °C for 2 h and precipitation annealing at 870 °C for 24 h. The structure of the investigated MAR-M 247 alloy is dendritic with coarse grains of average size 0.8 mm (determined by linear intercept method). Numerous casting defects were detected in the structure. Their typical size was around 400 μm. The

✉ M. Šmíd
smid@ipm.cz

¹ Institute of Physics of Materials, Academy of Sciences of the Czech Republic, Žitkova 22, 616 62 Brno, Czech Republic

² CEITEC IPM, Žitkova 22, 616 62 Brno, Czech Republic

³ Brno University of Technology, Technická 2, 616 69 Brno, Czech Republic

⁴ První brněnská strojírna Velká Bíteš a.s., Vlkovská 279, 595 12 Velká Bíteš, Czech Republic

strengthening phase γ' with the volume fraction around 60 % is heterogeneously distributed in the γ matrix. Areas of fine γ' precipitates with mostly cuboidal shape (edge size 0.4 μm) are often surrounded by areas of coarse γ' precipitates (1.6 μm in diameter) of more complicated morphology. Numerous carbides and eutectics γ/γ' were found in the interdendritic and grain boundary areas (see Fig. 1).

A resonant testing machine with 100 kN force range was used for fatigue tests under load control in fully reversed loading (stress ratio $R = -1$). The frequency of cyclic loading was around 120 Hz. Cylindrical specimens with a gauge length of 8 mm in diameter and 23 mm in length were used for experimental determination of the fatigue life. The temperature of testing was provided by a furnace with resistance heating. All tests were done in laboratory air. The tests were terminated when the frequency decreased by 5 Hz or in the case of specimen rupture. The fracture surfaces and specimen cross-sections were investigated by scanning electron microscopy (SEM). Selected fractured specimens were sectioned longitudinally with the loading axis by electroerosion cutting and carefully prepared for EBSD analysis of grains nearby the fracture surface.

3 Results

3.1 S–N Curves

Figure 2 shows S–N curves of the MAR-M 247 alloy corresponding to the fully reversed cyclic loading at four

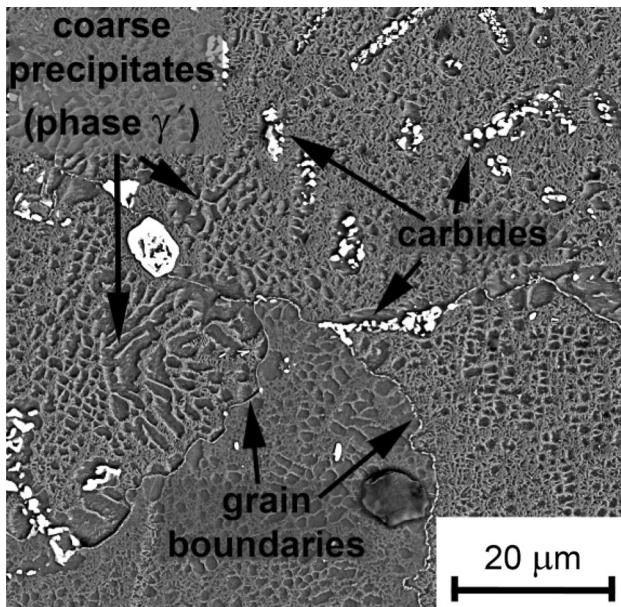


Fig. 1 Microstructure of MAR-M 247 with main structural features

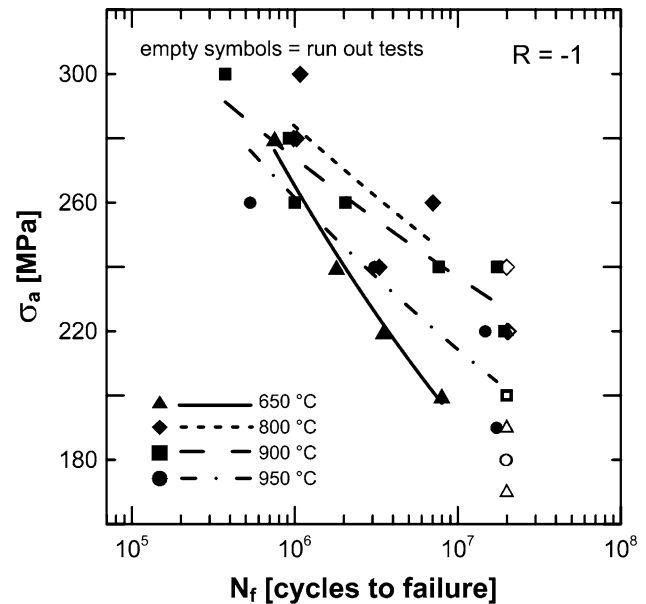


Fig. 2 HCF data of MAR-M 247 at four experimental temperatures. Empty symbols denote unbroken specimens

temperatures. Experimental data exhibit significant scatter due to coarse dendritic structure of the alloy. Another reason for the scatter is a random size and density of shrinkage pores present in bulk of the material. These two factors generate a situation when the fatigue life of two specimens tested on the same stress amplitude differs by more than one order of magnitude. The diagram indicates that the slopes of the S–N curves at temperatures 800, 900 and 950 °C are similar with consideration of possible scatter of the data. The curve representing fatigue tests at 650 °C exhibits significantly steeper slope.

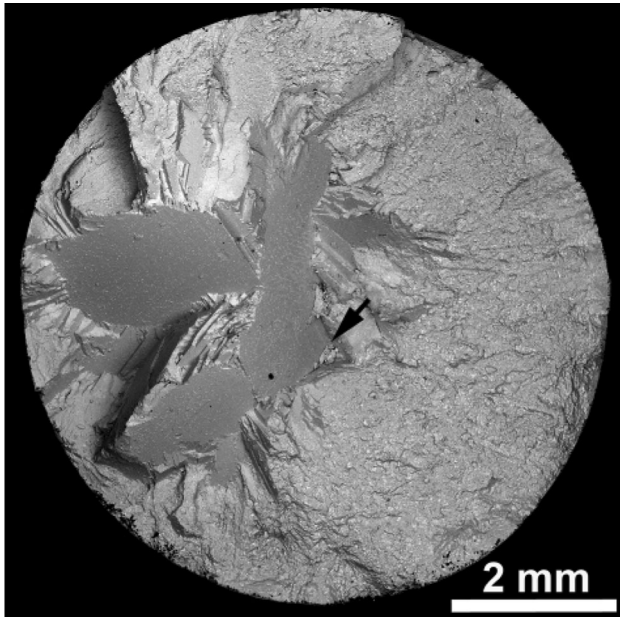
Experimentally determined values of the fatigue limit for each temperature are summarized in Table 1. The fatigue limit, σ_f , was defined as the stress amplitude at which a minimum of three specimens reached 2×10^7 cycles without failure. The temperature dependence of the obtained values of the fatigue limit correlates well with the typical yield strength anomaly observed for most of the nickel base superalloys. Relatively low fatigue limit was determined for 650 °C and simultaneously the S–N curve indicates very poor HCF performance. Contrary to that, the best HCF properties with the highest fatigue limit were found for 800 °C. Slow decrease of fatigue limit begins to emerge with temperature exceeding 900 °C. Nevertheless, the alloy exhibits quite good fatigue performance even at 950 °C.

3.2 Fractography

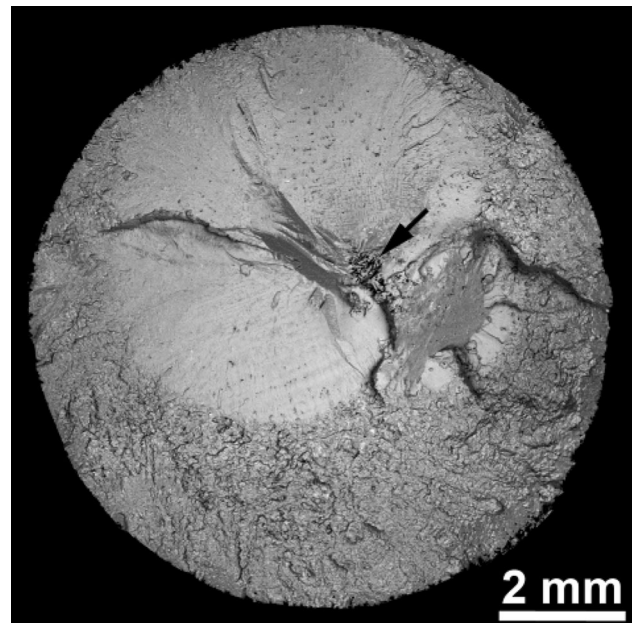
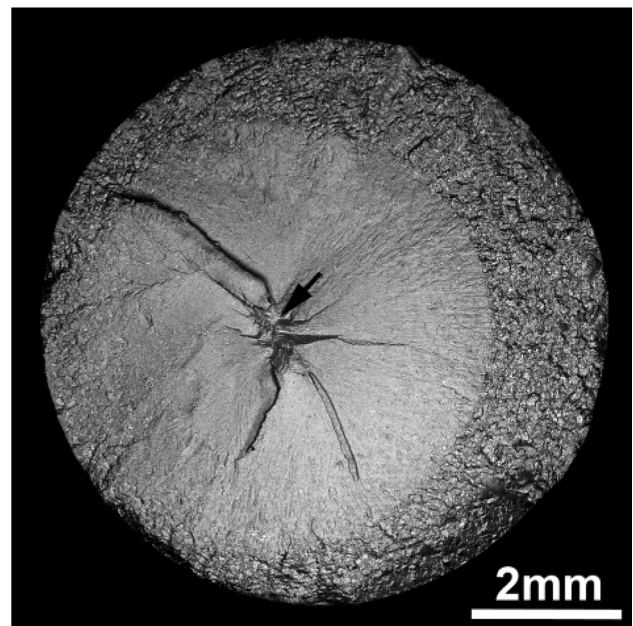
The fracture surface analysis was done on selected specimens with the aim to localize fatigue crack initiation sites

Table 1 Fatigue limits of the MAR-M 247 alloy at four experimental temperatures

Temperature (°C)	650	800	900	950
Fatigue limit σ_f (MPa)	190	220	200	180

**Fig. 3** Fracture surface with numerous facets. Fatigue fracture initiation site is marked by the arrow. Test temperature 650 °C

and to describe main features of the crack propagation. Figures 3, 4, 5 and 6 show SEM images of typical fracture surfaces after fatigue tests for each experimental temperature. It is obvious that the appearance of the fracture surface changes significantly with increasing temperature. Highly rugged fracture surface with numerous crystallographic facets inclined at various angles to the loading axis is characteristic for fatigue tests at 650 °C (see Fig. 3). Such features are typical for crystallographic mode of the fatigue crack propagation. This mode is prevailing from the crack initiation till the late stages of the fatigue life of the specimen. Only small fracture surface area before the final failure corresponds to the non-crystallographic propagation mode and exhibits striation fields. Large spacing of the striations indicates that this stage of propagation represented only a short period of the specimen fatigue life before its final fracture. Distinct change in appearance of the fracture surfaces was observed on specimens tested at 800 °C. The crystallographic mode of propagation was limited just on the areas in the vicinity of the crack initiation sites (see Fig. 4). Only some crystallographic facets are present on the fracture surface. The decisive rest of the fatigue life was characterized by the non-crystallographic

**Fig. 4** Fracture surface with few facets. Test temperature 800 °C**Fig. 5** Fracture surface with large fish eye. Test temperature 900 °C

crack propagation resulting in formation of striations, river patterns and beach marks.

Except of few rare facets present on fracture surface, disappearance of the crystallographic crack propagation mode and formation of fish eyes was observed on fracture surfaces of specimens tested at 900 °C (Fig. 5). Interdendritic regions rich in carbides were visible on the fatigue fracture surfaces. This indicates that the crack propagates along the interdendritic areas and along the grain

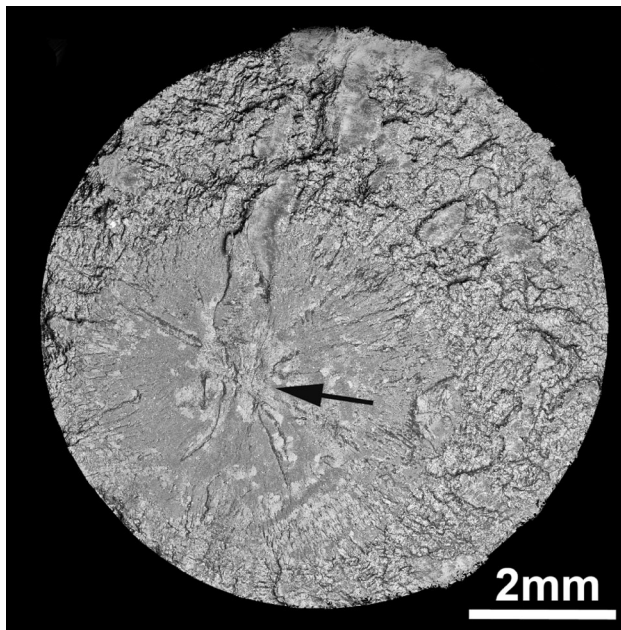


Fig. 6 Severely oxidized fracture surface. Test temperature 950 °C

boundaries. Similar observation was made on the specimens tested at 950 °C. Significantly higher oxidation was apparent when compared to 900 °C. The fatigue crack initiation mostly occurred in the vicinity of shrinkage pores which act as the stress concentrators. In several cases, the fatigue crack initiation from the specimen surface was observed. Shrinkage pores were found in these cases in the initiation region.

3.3 EBSD Analysis

The EBSD analysis results conducted on the gauge length of specimens sectioned parallel to the loading axis are shown in the Figs. 7 and 8. The analysis was conducted in areas under the fracture surface with the aim to bring more insight into the observed transition from the crystallographic to the non-crystallographic crack propagation. The cross-sections were made near or across the areas of the crack initiation. Inclination angle to the loading axis and Schmid factors of given planes were calculated from the recorded EBSD data. Only the planes of the type $\{111\}$ were taken into account due to the FCC lattice of studied material.

The EBSD analysis of the fatigue crack propagation at temperature 650 °C is shown in Fig. 7. In this particular case the fatigue crack initiated in the coarse grain no. 1. Crystallographic propagation took place across the whole grain and was over 3 mm long. The results of the EBSD analysis of neighbouring grains marked by numbers are shown in the figure. The crack propagated along the plane (111) in early stage of the fatigue life. The trace of the

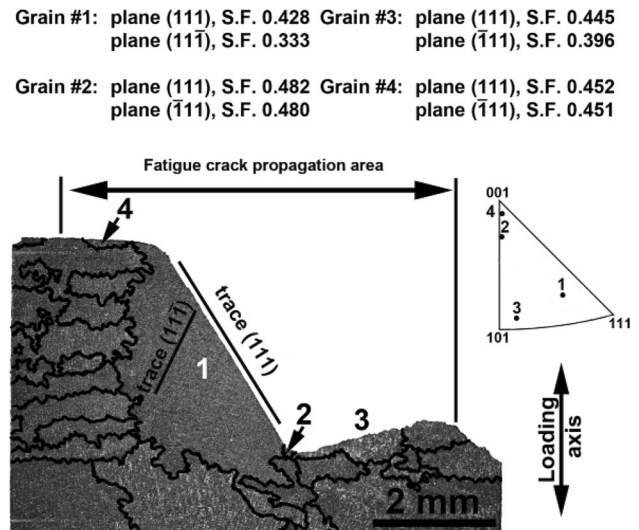


Fig. 7 The EBSD analysis of specimen longitudinal section. Test temperature 650 °C

Grain #1: plane (111), S.F. 0.464	Grain #3: plane (111), S.F. 0.473
plane $(\bar{1}\bar{1}\bar{1})$, S.F. 0.348	plane $(\bar{1}\bar{1}1)$, S.F. 0.368
Grain #2: plane (111), S.F. 0.481	Grain #4: plane (111), S.F. 0.449
plane $(\bar{1}\bar{1}\bar{1})$, S.F. 0.4240	plane $(\bar{1}\bar{1}1)$, S.F. 0.422

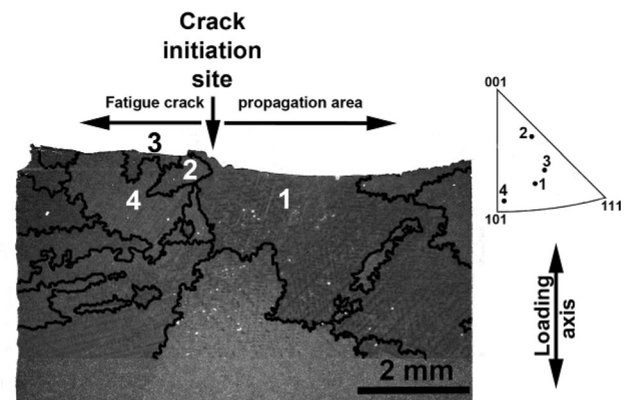


Fig. 8 The EBSD analysis of specimen longitudinal section. Test temperature 900 °C

plane is highlighted in the figure along with the trace of plane $(\bar{1}\bar{1}\bar{1})$ which had the second highest Schmid factor. It can be seen that despite some well-oriented planes in remaining grains with high Schmid factors the fatigue crack propagated further in the non-crystallographic mode.

Another EBSD analysis (Fig. 8) was conducted on the cross-section of specimen after cyclic test at 900 °C. The section was made again in the vicinity of the crack initiation site. Fracture surface profile is without any evidence of crystallographic facets and the entire fatigue crack propagation corresponds to the non-crystallographic mode. It should be remarked that this mode appeared despite the fact that the investigated grain is oriented to the loading

axis in similar manner like in case of the specimen cycled at 650 °C. Note, that dimensions of both grains are similar.

4 Discussion

HCF tests done in range from 650 to 950 °C have shown significant changes of the crack propagation mode with temperature. The fatigue fracture surfaces after cyclic tests at 650 °C and partially 800 °C exhibit brittle-like morphology with numerous crystallographic facets. Along with this finding, the S–N curve obtained at 650 °C has different slope from the curves determined at higher temperatures. Therefore the crack propagation mode has substantial importance for HCF performance of the superalloys.

Determining factor for such behaviour is low stacking fault energy of this group of materials. The main consequence is difficult cross-slip of mobile dislocation during high temperature loading. Therefore the cyclic plastic deformation is localized predominantly into narrow slip bands of some {111} planes as it was already documented by several studies [7–9] at various loading conditions and temperatures. Such degree of heterogeneous cyclic plastic deformation distribution in material leads to the crack initiation and subsequently the crack propagation along these activated planes. On the account of this, the crack propagation is highly crystallographically dependent especially at temperature 650 °C. This dependency was confirmed by the EBSD analysis in presented study (see Fig. 7). It has been found that suitably oriented large grain with stress concentrator like shrinkage pore in its vicinity is the predominant area of the crack initiation. The initiation takes place on some of {111} planes with the highest Schmid factor and continue to propagate along till reaching of a grain boundary.

With increasing temperatures the importance of additional phenomena on fatigue behavior is gradually rising. Dislocation mobility increases rapidly due to pronounced thermally activated processes like diffusion and dislocation climb. Therefore, planarity of the cyclic plastic deformation and the related crystallographic mode of the fatigue crack propagation decrease significantly. This fact was illustrated by reduced appearance of crystallographic facets on the fracture surface of the specimen tested at 800 °C (Fig. 4). Above 800 °C, the planar localization of the cyclic plastic deformation disappeared entirely according to the EBSD results. Despite well-oriented large grain (Fig. 8) which contained shrinkage pores, no evidence of the crystallographic crack propagation was observed. Carbides and the interdendritic areas became more favorable for the crack propagation along with the transition to the non-crystallographic mode. The observed decrease of the fatigue performance at 950 °C can be addressed to the

environmental influence. It was proved, e.g. in [10], that oxidation damage can accelerate the fatigue crack growth rate and subsequently shortens the fatigue life.

5 Conclusions

1. The S–N curve of MAR-M 247 alloy at 650 °C has steeper slope than the S–N curves corresponding to higher temperatures due to dominant crystallographic mode of the crack propagation. The S–N curves measured at 900 and 950 °C have nearly similar slope reflecting non-crystallographic crack propagation observed at these temperatures. The slope of the S–N curve at 800 °C does not differ from the fatigue life curves at 900 and 950 °C despite the fact that crystallographic mode of the crack propagation was active in early stages of the fatigue life.
2. The highest fatigue limit (based on 2×10^7 cycles) was found at the temperature of 800 °C.
3. The most frequent fatigue crack initiation site is internal initiation from shrinkage pores. In the case of extremely low porosity of material the initiation of cracks took place on the surface.
4. The EBSD analysis confirmed crystallographic dependency of the damage mechanisms at 650 °C. The cracks follow strictly {111} type slip planes. These crystallographic features of the crack growth were not found at 900 °C.

Acknowledgments Authors of the article are grateful for financial support by the Project TA04011525 Technological Agency of the Czech Republic. This work was realized in CEITEC—Central European Institute of Technology—with research infrastructure supported by the Project CZ.1.05/1.1.00/02.0068 financed from European Regional Development Fund.

References

1. Szczotok A, Szala J, Cwajna J, Hetmańczyk M, *Mat Char* **56** (2006) 348.
2. Liao J-H, *Mat Trans* **52** (2011) 201.
3. Gelmedin D, and Lang K H, *Int J Mat Res* **103** (2012) 97.
4. Boismier D A, and Sehitoglu H, *J Eng Mater T ASME* **112** (1990) 68.
5. Bor H Y, Hsu C, Wei C N, *Mat Chem Phys* **84** (2004) 284.
6. Šmíd M, Kunz L, Hutař P, Hrbáček K, *Proc Eng* **74** (2014) 329.
7. Yi J Z, Torbet C J, Feng Q, Pollock T M, Jones J W, *Mat Sci Eng A* **443** (2007) 142.
8. Petretec M, Obrtlík K, Polák J, *Mat Sci Eng* **400–401** (2005), 485.
9. MacLachlan D W, and Knowles D M, *Fatigue Fract Eng M* **24** (2001) 503.
10. Pineau A, in *Mechanical Behaviour of Materials at High Temperature*, (eds) 1996, Branco Moura C, Ritchie R, Sklenička V, Springer, Netherlands, (1996) p 135.